Ab initio approach to photostriction in classical ferroelectric materials

Charles Paillard, Sergey Prosandeev, and L. Bellaiche

Phys. Rev. B **96**, 045205 — Published 25 July 2017

DOI: 10.1103/PhysRevB.96.045205

Ab-initio Approach to Photostriction in Classical Ferroelectric Materials

Charles Paillard,[1] Sergey Prosandeev,[1,2] and L. Bellaiche[1]

[1] *Department of Physics and Institute for Nanoscience and Engineering, University of Arkansas, Fayetteville, AR 72701, USA*

[2] *Institute of Physics and Physics Department of Southern Federal University, Rostov-na-Donu 344090, Russia*

(Dated: July 5, 2017)

The change of shape under illumination by visible light, called photostriction, is investigated in the classical ferroelectrics barium titanate and lead titanate. By means of the ΔSCF method, the use of first-principle calculations confirms that the converse piezoelectric effect is the main driving force of the photostriction of the polar axis in those materials. As a result, when compared to barium titanate and bismuth ferrite, lead titanate is a better photostrictive material in the direction of the polar axis, due to its larger longitudinal piezoelectric constant. On the other hand, in directions transverse to the polar axis, photo-induced electronic pressure can also become a sizable contribution that can either compete or cooperate with the piezoelectric effect, depending on the transitions involved. A simple Landau model is further developed and shows reasonable qualitative agreement with results from ΔSCF calculations, which is promising for a fast screening of materials with high photostrictive effects.

PACS numbers: 77.65.-j,78.20.H-,78.20.Pa

I. INTRODUCTION

Photostriction is the strain induced in a material under illumination. Interest in that effect has been aiming so far at designing devices exploiting the coupling of light and strain. It was proposed (and demonstrated) as early as the 1990's that photostriction could be applied to the design of optically controlled relay, micro-walking robots or photophones using PLZT-based bimorph structures[1]. More recently, the generation of acoustic waves in pump-probe experiments[2–4] may drive the development of ultra-fast, optically controlled, acoustic transducers. Similar experiments have shown the possibility of generating strong strain gradients in bismuth ferrite thin films[5], opening the way to a possible optical control of polarization switching or domain writing through the flexoelectric effect[6]. The interplay of strain and magnetic degrees of freedom through magneto-elastic couplings has also been used recently in order to control optically the magnetic hysteresis loop of a nickel film deposited on top of a bismuth ferrite crystal[7].

So far most works on photostriction have been based on experiments. Being able to employ first-principles in order to investigate and predict photostriction phenomena is important, in order to, e.g., design efficient photostrictive materials, or for instance assess the impact of defects and domain walls on photostrictive properties. Also, disentangling which mechanism between thermal dilatation caused by sample heating when light is absorbed, potential deformation (the strain generated by the electronic redistribution of photo-excited carriers), electrostriction (the quadratic response of strain to an electric field) or piezoelectricity[8,9] is the main driving force of photostriction is a critical step to tailor the photostrictive properties of a material. As a first step towards that goal, we recently presented a work employing the ΔSCF method to describe photostriction in bismuth ferrite[10]. It was proposed that the piezoelectric effect is the main driving force of photostriction in such material. Although bismuth ferrite has been the most studied material with respect to photostriction due to its relatively small bandgap as compared to other common ferroelectric materials, it has a relatively small piezoelectric constant ($d_{33} \approx 25 - 70$ pC.N^{-1} according to calculations[11] and experiments[12]). To compare with, single crystals of barium titanate have been measured to have a piezoelectric constant d_{33} of 85.6 pC.N^{-1} at room temperature[13], and lead titanate-lead magnesium niobate solid solution have piezoelectric constants that can exceed 1000 pC.N^{-1} near their Morphotropic Phase Boundary[14]. A recent computational work on 2D monochalcogenides films has further shown that, owing to their significant piezoelectric constants, a larger photostriction effect than in $BiFeO_3$ was expected in these films[15] . Although such ultra-thin films may be appealing for their potential ultrafast response time, their integration in actual devices may be challenging. The pursuit of highly photostrictive bulk materials must therefore continue. The ability to understand the origin of photostriction in terms of simple concepts (piezoelectricity *vs* electronic pressure), and the ability to design simple analytical models to quickly screen for high photostrictive materials, are key milestones in the pursuit of this goal. As a step towards these objectives, we used here the ΔSCF method, which is detailed in Section II alongside technical details. The following Section III demonstrates that the classical ferroelectric oxides barium and lead titanates show appreciable photostrictive behavior. The mechanisms ruling photostriction in those materials are then revealed and discussed in Section IV, and a Landau model of photostriction is then developed and detailed as a qualitative tool for the prediction of photostriction from ground-state calculations. Finally, Section V concludes this work.

II. METHODS

A. The ΔSCF method

When performing Density Functional Theory (DFT) calculations, one is typically minimizing the energy functional with respect to density by self-consistently resolving the ground state density, in accordance with the two Hohenberg-Kohn theorems at the foundation of DFT[16]. There are several schemes to achieve such calculations, however one simple, popular and practical way is to assume that one can find a system of non-interacting electrons with the same energy and ground state density as the true system of fully interacting electrons. Such approximation is called the Kohn-Sham (KS) ansatz[17], and provides us with a physically intuitive one-electron picture, within which one is left to fill monoelectronic orbital states (determined from a monoelectronic Schrödinger equation) by increasing levels of energy. As described in Fig. (1), a KS calculation would start by guessing an input potential V_{in}, thereby fully determining the one-electron Hamiltonian. This Hamiltonian is then solved, resulting in a set of monoelectronic orbitals φ_i with eigenvalues ε_i. The lowest energy lying states would then be filled in order to determine the ground state, and the new potential V_{out} generated by the distribution of electrons in these occupied orbitals becomes the input for a new cycle, until convergence of the ground state density is reached up to a desired accuracy.

The ΔSCF method[18] is essentially analog to a regular Kohn-Sham calculations: starting from an input potential V_{in}, the monoelectronic Schrödinger equation is solved. The main difference arises when the filling of the orbitals is performed. As sketched in Fig. (1.b), some electrons are constrained to occupy excited states in the conduction band, while leaving holes in the valence band. Therefore, the system is converged under the constraint of having some electrons lying in higher energy states, and holes in lower energy states. This rather simple approach has proved rather successful in describing resonance level in finite systems such as molecules adsorbed on metallic surfaces[19], or the ligand-field splitting in Fephtalocyanine[20]. In infinite systems however, the ΔSCF method does not improve much the description of excited states energies such as the bandgap energy when using traditional functionals[21]. One should resort to more accurate models, such as the *GW* approximation[22] or Time Dependent DFT (TD-DFT)[23], which are rather computationally expensive. Nevertheless, since our main focus is photostriction, we are not particularly interested in excitation energies, but rather into the relaxation of the lattice under excitation. Furthermore, we note that many *GW* calculations are typically used as corrections to eigenenergies and wavefunctions determined with a more traditional functional[24]. Thus, we consider the ΔSCF method as being a good approximation for our purpose, as it has given reasonable values for photostriction compared to experiment in earlier works[10].

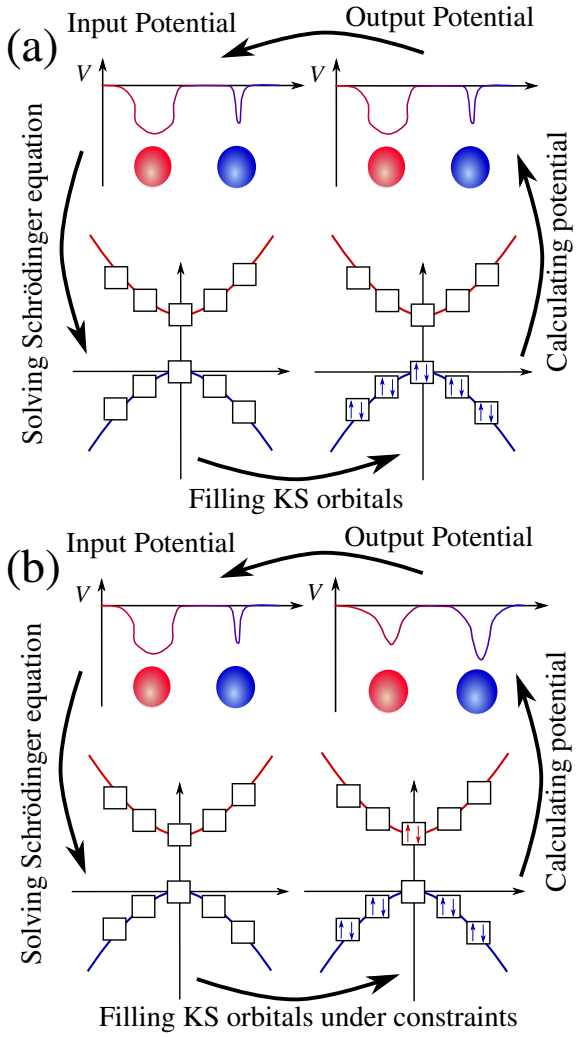

FIG. 1. (a) Regular Kohn-Sham calculation to find the ground state electronic density: from an input potential V_{in}, the now known Kohn-Sham Hamiltonian can be diagonalized. Its lowest eigenstates ("orbitals") are then filled with electrons, and a new potential is calculated based on the latter electronic distribution. The output potential is then plugged in as input potential until convergence to a reasonable accuracy is reached. (b) ΔSCF calculation: at filling, not all low energy lying eigenstates are filled, but some electrons are imposed to occupy excited orbitals. An output potential is then calculated based on this electronic distribution, and the density is self-consistently solved under the constraint of certain occupation numbers.

B. Computational details

As mentioned in the introduction, we consider barium and lead titanates, of formula unit $BaTiO_3$ and $PbTiO_3$, respectively. We use the Abinit[25] plane-wave code with the PAW method[26,27] to describe those two materials. As shown in previous studies, the Local Density Functional (LDA) functional[17,28] captures most physical traits of those materials[29,30], and is in particu-

	LDA This work	PBESol This work	LDA Ref.[32]	GGA Ref.[33,a]	HSE06 Ref.[34]	Exp. Ref.[35]
a (Å)	3.8693	3.8882	3.86	3.892	3.855	3.904
c/a	1.0455	1.0739	1.047	1.073	1.071	1.065
δz_{Ti}	-0.0322	-0.0385	-0.0348	-0.030		-0.038
δz_{O_1}	-0.1011	-0.1183	-0.1035	-0.110		-0.112
δz_{O_3}	-0.0895	-0.1104	-0.0922	-0.105		-0.117

TABLE I. Summary of structural parameters in $P4mm$ $PbTiO_3$: basal lattice constant a, c/a ratio, and shift of the ions with respect to lead, given in units of the tetragonal axis c.

	LDA, This Work	LDA	Expt. [a]
a_{BTO} (Å)	3.9462	3.943[30]	3.980[36]
a_{PTO} (Å)	3.8950	-	3.926[37]

TABLE II. Lattice constant of the $Pm\bar{3}m$ high temperature phase of $BaTiO_3$ (BTO) and $PbTiO_3$ (PTO).

lar able to describe their ground state as polar, of symmetry $R3m$ and $P4mm$, respectively. The plane wave cut-off was taken as 952 and 1088 eV for $BaTiO_3$ (BTO) and $PbTiO_3$ (PTO). We used non-shifted $16 \times 16 \times 16$ and $18 \times 18 \times 18$ k-meshes respectively. The use of a non-shifted grid is required to retain the high-symmetry points of the band structure, which are usually local extrema. During Self-Consistent Field (SCF) calculations, the density was considered converged when the difference of the forces on the ions between two SCF iterations did not exceed 5×10^{-7} eV.Å^{-1}. Subsequently, the structural relaxation (both ionic positions and cell shape) was considered achieved when the maximum force on the ions was smaller than 2.6×10^{-5} eV.Å^{-1} and the stress tensor components smaller than 1.5×10^{-3} kbar. Such strict convergence criteria was necessary to avoid physically wrong results, especially at small concentration of excited electrons. Overall, the large plane-wave cut-off, dense k-meshes, and strict convergence criteria ensure that lattice constants are converged to less than 10^{-3} %, which is necessary given how small the photostriction effect is, experimentally, in bulk materials (typically, $\frac{\Delta L}{L} \approx 10^{-2} - 10^{-4}$ %[8,31]). Note that, in the case of lead titanate, calculations using the PBESol functional were also carried out to check the influence of the functional on the results. Both the ground states ($R3m$ and $P4mm$, respectively) and the paraelectric $Pm\bar{3}m$ phase of barium and lead titanates were investigated, in order to compare the respective magnitude of the piezoelectric and potential deformation effects as driving force of photostriction in these materials. The structural parameters for the four structures considered in this work are summarized in Tables I, II & III. Overall, the agreement with previous works is rather good, and the lattice constant calculated within LDA underestimates the experimental values by 1-2 % as expected.

	LDA This work	LDA Ref.[30]	Exp. Ref.[38]
a (Å)	3.9594	4.001	4.0036
α (°)	89.91	89.87	89.839
δx_{Ti} (units of a)	-0.0100	-0.0110	-0.0128
δx_{O_3} (units of a)	0.0098	0.0133	0.0109
δz_{O_3} (units of a)	0.0152	0.0192	0.0193

TABLE III. Lattice constant of the $R3m$ rhombohedral phase of $BaTiO_3$, and displacement of ions from their ideal position along the pseudo-cubic axes with respect to the barium ion.

C. Band structure and considered transitions

Band structure dispersion curves were generated, and are plotted in Fig. (2). The band structure of lead titanate in its ground state phase, depicted in Fig. (2.a), shows two main valleys in the valence band, at the $X = (1/2, 0, 0)$ and $Z = (0, 0, 1/2)$ points located the edges of the Brillouin zone. Overall, the X point is the top of the valence band, while the Z point, in the tetragonal direction, has a slightly lower energy. The bottom of the conduction band is made by the Z and Γ points, and the dispersion along the path joining those two points is quasi-flat, indicating strong localization onto the titanium d-states. When moving to the centrosymmetric cubic phase $Pm\bar{3}m$, plotted in Fig. (2.b), one observes that Z and X have degenerate energies, which is expected owing to the recovered cubic symmetry. The Kohn-Sham bandgap is respectively indirect ($X \rightarrow Z$) with value 1.49 eV, and direct ($X \rightarrow X$ and $Z \rightarrow Z$) with value 1.45 eV for the $P4mm$ and $Pm\bar{3}m$ structures.

The cubic structure of barium titanate has a band structure (in Fig. (2.c)) fundamentally different from that of lead titanate, because of the presence of the lead $6s^2$ lone pair of the former, as noted by Erhart *et al.*[40]. In $BaTiO_3$, valleys in the valence band are located at the Γ and R points, while the bottom of the conduction band is at Γ. The Kohn-Sham bandgap of the $Pm\bar{3}m$ structure is indirect ($R \rightarrow \Gamma$), with a value of 1.71 eV. The $R3m$ structure also has an indirect Kohn-Sham bandgap ($Z \rightarrow \Gamma$) of 2.06 eV. Note that in the Brillouin zone of the rhombohedral cell, $Z = (1/2, 1/2, 1/2)$, and therefore lies in the direction of the polar axis. For more information about the Brillouin zone of the different structures, the reader can refer to Ref.[39].

During our calculations, we typically fill some valleys in the conduction band with electrons, and some holes in the valleys of the valence band. We call "transition $A \rightarrow B$" when some holes are constrained to be in the valence band at the point A in the Brillouin zone and electrons are constrained at B in the conduction band. Such "transitions", depicted in Fig. (2), are: $Z \rightarrow Z$, $Z \rightarrow \Gamma$, $X \rightarrow \Gamma$ and $X \rightarrow Z$ for $PbTiO_3$ in the ferroelectric phase, $X \rightarrow X$ and $X \rightarrow \Gamma$ in the $Pm\bar{3}m$ phase, $\Gamma \rightarrow \Gamma$ and $R \rightarrow \Gamma$ for $Pm\bar{3}m$ barium titanate, and $Z \rightarrow \Gamma$ and $\Gamma \rightarrow \Gamma$ for rhombohedral $BaTiO_3$. Note

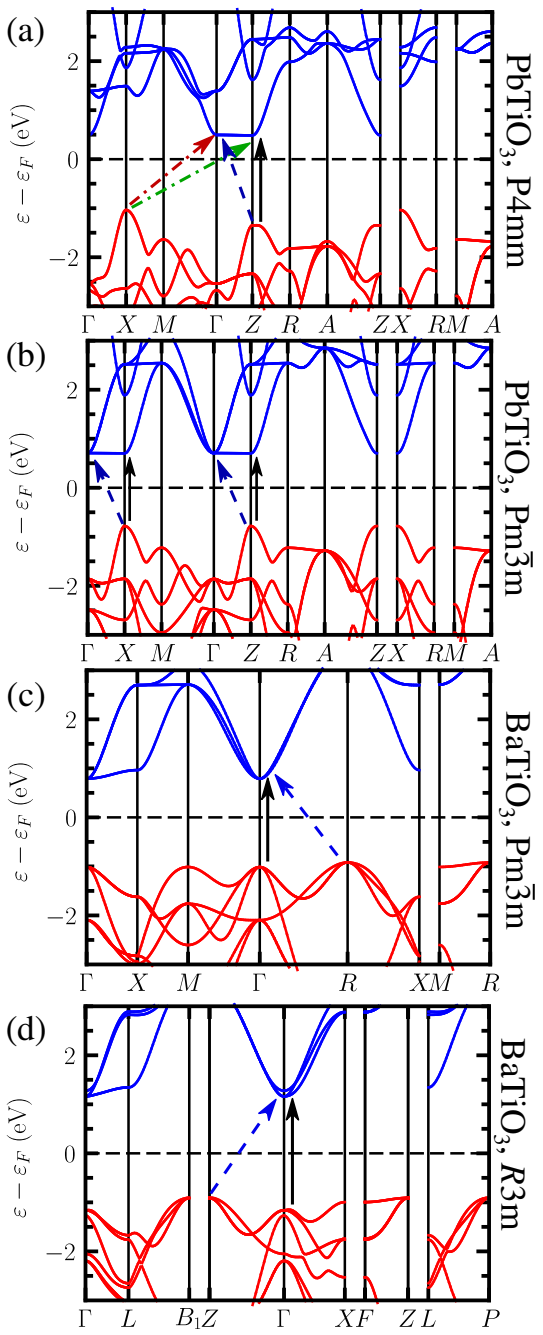

FIG. 2. Band structure of $PbTiO_3$ in the $P4mm$ ferroelectric (a) and $Pm\bar{3}m$ paraelectric (b) phases, and $BaTiO_3$ in the paraelectric $Pm\bar{3}m$ (c) and ferroelectric $R3m$ (d) states. Definition of k-points used can be found in Ref.[39] Arrows represent the different "transitions" considered here.

that those are not necessarily optical transitions. Our assumption here is that the electron-phonon interaction, which thermalizes the photoexcited electrons and relax them to the lowest energies of the conduction band, is fast enough compared to the recombination time of the electron-hole pair. As a result, we fill only valleys with electrons and holes in the conduction and valence bands. According to Ref.[9], the relaxation time of the electron to the bottom of the conduction band is typically of the order of 1 ps, while recombination has a much larger (1 ns-1 μs) relaxation time, justifying this approximation. Note that, therefore, we are only concerned with steady photostriction here, and do not investigate the ultra-fast response observed in picosecond or sub-picosecond pump-probe experiments[41–44].

Eventually, note that we determine the concentration of photoexcited electrons, denoted n_e, by summing over the electronic population of different $k-$points in the the conduction band,

$$n_e = \frac{1}{V_0} \sum_{\boldsymbol{k}} w_{\boldsymbol{k},\mathrm{CB}} n_{\boldsymbol{k},\mathrm{CB}}, \tag{1}$$

with V_0 being the volume of the unit cell in the ground state, $w_{\boldsymbol{k},\mathrm{CB}}$ the weight of the k-point $\boldsymbol{k}$ in the Brillouin zone, and $n_{\boldsymbol{k},\mathrm{CB}}$ the number of electrons in the conduction band with wavevector $\boldsymbol{k}$.

III. RESULTS

In the following section, we present the results obtained from our ΔSCF calculations.

A. Photostriction in the ferroelectric ground state

In ferroelectric lead titanate, we considered the four transitions $Z \to Z$, $Z \to \Gamma$, $X \to \Gamma$ and $X \to Z$. The results, presented in the right panel of Fig. (3), show that for all considered transitions, the c axis of the unit cell shrinks linearly with increasing concentration of photoexcited electrons n_e. Interestingly, among the two investigated position of the photoexcited electron in the Brillouin zone, Z and Γ, no major difference is found in the photo-induced change of lattice constants, most likely due to the very similar nature of the involved conduction states, which are both d-orbitals located on titanium (see Kohn Sham states of the conduction band depicted in Fig. (4)). Rather, the position of the hole, whether it is placed at X or Z, results in drastically different results: the change in the c axis lattice constant is six times larger if the photoinduced hole sits at the Z point rather than at the X point. In addition, the basal lattice constant a *increases* when the hole is placed at Z, but slightly decreases when placed at X. Looking at the nature of the states involved in Fig. (4), one notes that the valence Kohn-Sham state at X involves the four oxygens perpendicular to the x direction, with $2p_x$ orbitals. On the contrary, the valence band Kohn-Sham state at Z only includes the four oxygen lying in the plane orthogonal to the tetragonal axis, with lobes *pointing along the tetragonal axis*.

In ferroelectric barium titanate, the investigation of the two transitions $\Gamma \to \Gamma$ and $Z \to \Gamma$ show that in both

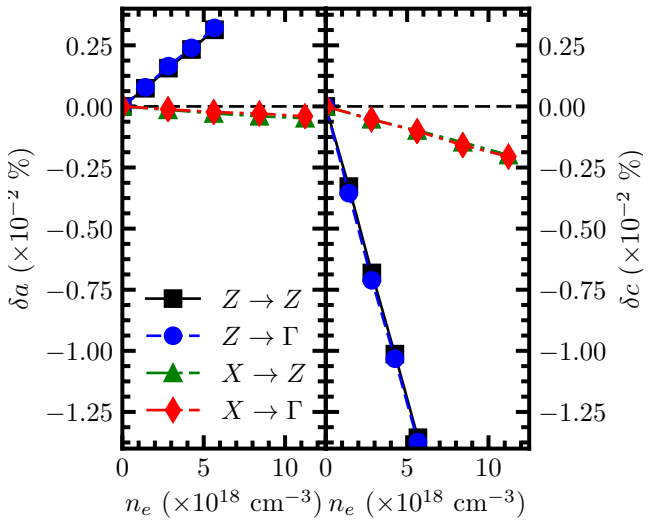

FIG. 3. Evolution of the a (left panel) and c (right panel) lattice constants in ferroelectric lead titanate for $Z \to Z$ (black squares), $Z \to \Gamma$ (blue circles), $X \to Z$ (green triangles) and $X \to \Gamma$ (red diamonds).

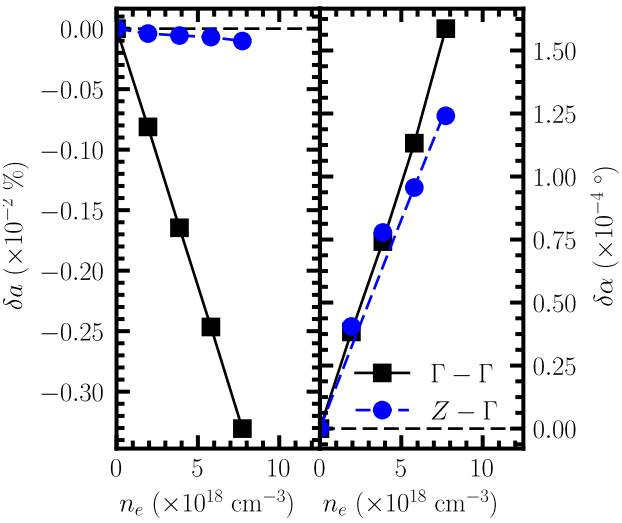

FIG. 5. (left panel) The pseudo-cubic lattice constant a of rhombohedral barium titanate decreases with increasing concentration of photoexcited electrons n_e, for both transitions. (right panel) Concurrently, the pseudocubic angle α increases.

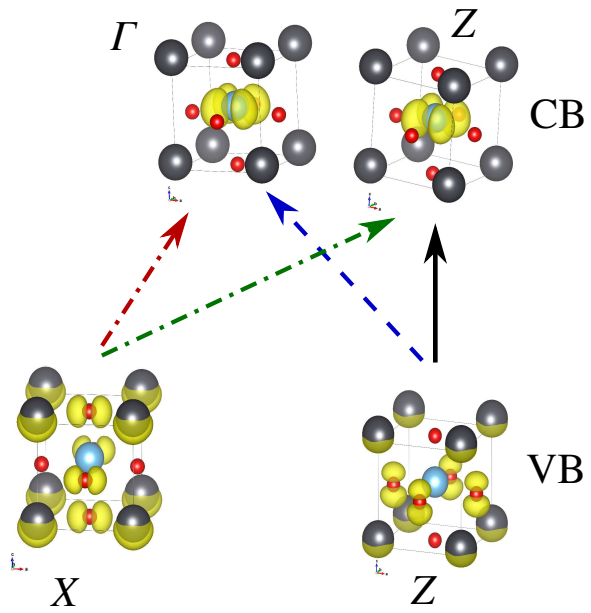

FIG. 4. 10% isosurface of the amplitude of the monoelectronic wavefunctions for states in the valence band located at X and Z in the Brillouin zone, and in the conduction band at Z and Γ, in tetragonal lead titanate.

cases, the pseudo-cubic lattice constant of the five atom unit cell decreases with increasing n_e, but the decrease is more than 15 times larger in the case of the $\Gamma \to \Gamma$ transition, as shown in the left panel of Fig. (5). The right panel of the same figure shows that the pseudocubic angle α increases towards 90° with rather similar rate for both transitions. The decrease of the pseudocubic lattice constant, with an increasing pseudocubic angle, is a feature that was already observed in rhombohedral bismuth ferrite[10].

Note that, in the case of lead titanate, the change of lattice constant along the tetragonal axis is potentially stronger than in barium titanate; at least the $Z \to Z$ transition considered in lead titanate leads to a photostrictive effect that is at least 3 times as large than that of the $\Gamma \to \Gamma$ transition in $BaTiO_3$.

B. Photostriction in the paraelectric phase

In order to probe how important is the existence of the polarization and related properties such as piezoelectricity, we also performed ΔSCF calculations on the high-symmetry paraelectric $Pm\bar{3}m$ phase of lead and barium titanates.

Let us start with $BaTiO_3$. As shown in Fig. (6), upon increasing the number of electrons in the conduction band, the cubic phase of barium titanate *increases* its unit cell volume for the two valley transitions $\Gamma \to \Gamma$ and $R \to \Gamma$. In the case of lead titanate, the situation is opposite: both the $X \to \Gamma$ and $X \to X$ transitions lead rather to a *decrease* in volume.

Firstly, it is rather surprising that lead and barium titanates, two very similar compounds, *a fortiori* considered in the same $Pm\bar{3}m$ phase, exhibit so drastically different behaviors, one leading to an increase of lattice constant, the other to a decrease. In order to properly compare those two materials, we consider two additional transitions in the paraelectric cubic phase: $X \to \Gamma$ in $BaTiO_3$, and $\Gamma \to \Gamma$ for $PbTiO_3$. Figure (6) shows that

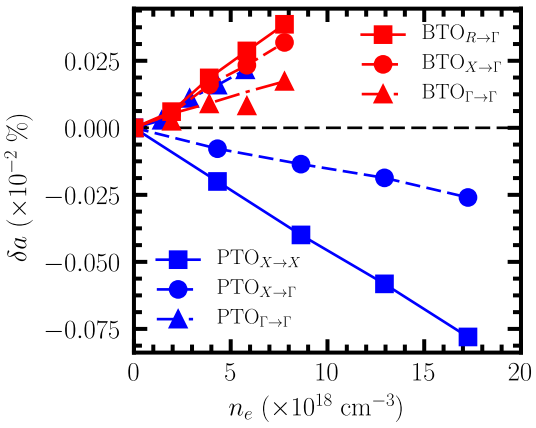

FIG. 6. Change of lattice constant of cubic $BaTiO_3$ (red) and cubic $PbTiO_3$ (blue) for different transitions.

Transition	$Pm3m$ $BaTiO_3$	$Pm3m$ $PbTiO_3$
$R \to \Gamma$	Increase	
$\Gamma \to \Gamma$	Increase	Increase
$X \to \Gamma$	Increase	Decrease
$X \to X$	-	Decrease

TABLE IV. Qualitative behavior of the lattice constant for various transitions in cubic paraelectric barium and lead titanates.

the $X \to \Gamma$ transition in $BaTiO_3$ has the same qualitative behavior as the $R \to \Gamma$ and $\Gamma \to \Gamma$ transitions, and causes BTO to expand. On the other hand, in lead titanate, the newly considered $\Gamma \to \Gamma$ transition presents an opposite behavior to that of the previous $X \to \Gamma$ and $X \to X$ transitions: now, the lattice constant is increasing with n_e. This is summarized in Table IV. Comparing Table IV and Fig. (7), in which the valence band states at Γ and X are depicted for both compounds, one immediately notices that, for the transition $X \to \Gamma$ which behaves oppositely in $BaTiO_3$ and $PbTiO_3$, there is a striking difference in the nature of the valence band state involved: at the X point, the lead atom $6s$ orbital hybridizes with the $2p$ orbitals of the oxygen atoms in lead titanate, while barium does not strongly hybridize with oxygen in barium titanate. On the contrary, at the Γ point in the valence band, neither $PbTiO_3$ nor $BaTiO_3$ exhibit hybridization of the A cation with oxygen, and both compounds show the same behavior in this case. One can therefore conclude that hybridization of the $6s$ orbital of lead with oxygen $2p$ orbitals is the driving force leading to a decrease of lattice constant with increasing concentration of excited carriers, while the absence of hybridization in $BaTiO_3$ leads to an opposite behavior.

Secondly, we observe that the reported change of lattice constant is one to two orders of magnitude smaller in the paraelectric phase compared to the ferroelectric phases of $BaTiO_3$ and $PbTiO_3$. The presence of polarization (and associated properties, such as piezoelectricity), is therefore an important factor in the deformation mechanism of ferroelectrics under illumination.

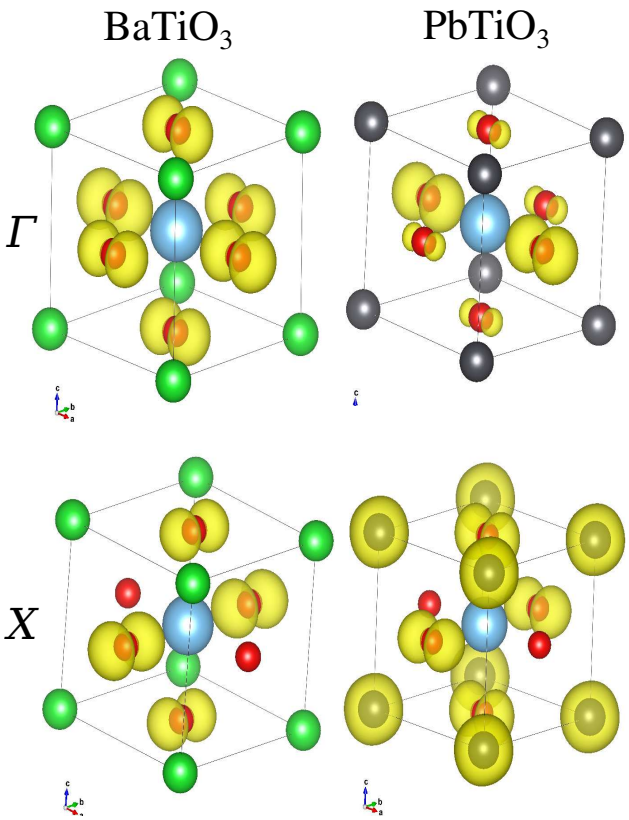

FIG. 7. Isosurface of the wavefunction amplitude of the valence band Kohn-Sham orbital at X and Γ for cubic $BaTiO_3$ (left) and $PbTiO_3$ (right).

C. Role of the functional: comparison LDA/PBESol

We also checked whether the results obtained using the LDA functional could be reproduced with the PBESol functional[45]. In the case of the PBESol exchange-correlation functional, we had to employ a plane-wave cut-off of 55 Ha, and a k-mesh of $20 \times 20 \times 20$ to ensure convergence of the ground state lattice constant with an accuracy of 10^{-3} %. The results, shown in Fig. (8), demonstrate that both the LDA and the PBESol functionals give qualitatively similar results. However, we note that the photostriction effect predicted in PBESol is typically larger than in LDA, and that it becomes nonlinear at large concentration of photoexcited carriers.

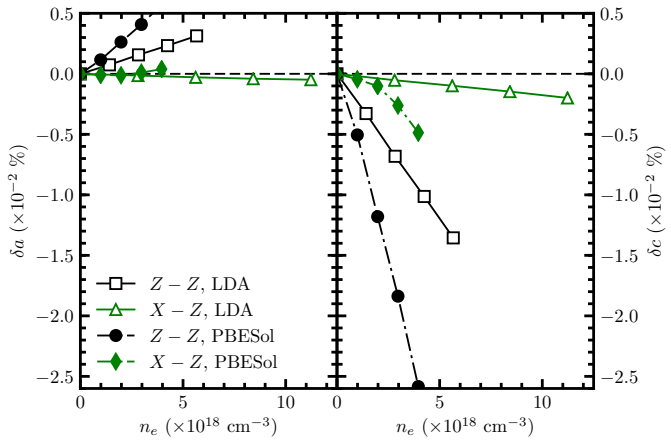

FIG. 8. Change of lattice constant δa and δc with increasing number of photo-excited electrons n_e in tetragonal lead titanate calculated from ΔSCF calculations, for LDA and PBESol functional.

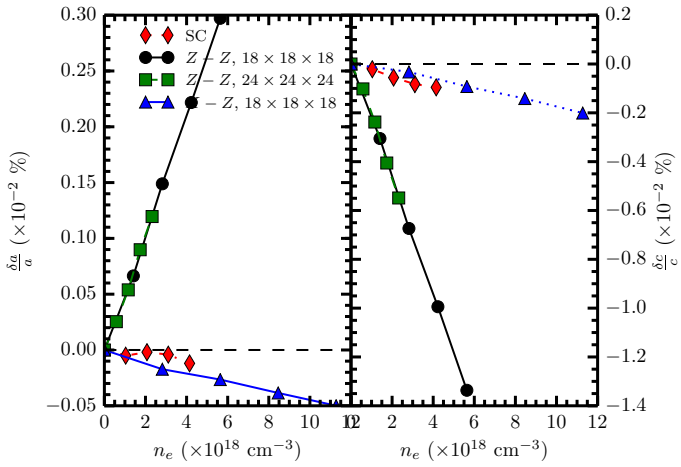

FIG. 9. ΔSCF calculations for two different k-meshes, and for a $2 \times 2 \times 2$ supercell (SC) calculated using a $9 \times 9 \times 9$ k-mesh, performed in $PbTiO_3$ in its $P4mm$ phase.

D. Influence of the cell size and k-mesh

We also tested how changing the k-mesh affects the results. Since the use of a $N_k \times N_k \times N_k$ mesh is equivalent to simulate a solid made of $N_k \times N_k \times N_k$ unit cells, being able to tune the k-mesh density is important if one wants to investigate a large range of concentration of photo-induced carriers. We therefore tested, on the $Z \rightarrow Z$ transition of tetragonal lead titanate, if the results with a $24 \times 24 \times 24$ k-mesh were consistent with our previous calculations using a $18 \times 18 \times 18$ k-mesh. Figure (9) shows that they are perfectly matching.

We also considered the case of $2 \times 2 \times 2$ supercell, with a $9 \times 9 \times 9$ k-mesh, in order to investigate the same range of concentration of photo-excited carriers as our calculations with a single unit cell and a $18 \times 18 \times 18$ k-mesh. We considered a $\Gamma \rightarrow \Gamma$ transition in the supercell, which, because of Brillouin zone folding of the band structure of the supercell, is equivalent to a $X \rightarrow Z$ transition in the unit cell. One can observe in Fig. (9) that the results in the supercell match rather well with the unit cell calculations.

IV. DISCUSSION

As mentionned in the Introduction, photostriction is the change of shape induced under illumination. One obvious contribution to photostriction is of thermal origin that is sample heating caused by illumination generates thermal dilatation, and has been ruled out as the main cause of photostriction in ferroelectrics[53]. There are however other significant contributions to the photostrictive properties of a material which are essentially non-thermal, such as potential deformation (the strain generated by the electronic redistribution of photo-excited carriers), or the electrostriction and piezoelectric effects (quadratic and linear response of strain to change in polarization)[8,9]. In particular, polar materials are particularly suited to control the shape of a material with light. Owing to their non-centrosymmetric nature, they are piezoelectric and naturally exhibit a Bulk Photovoltaic Effect (BPVE)[46–51]. As a result, the photo-induced change in polarization creates another source of stress mediated by the converse piezoelectric effect. Such mechanism is considered to be the main driving force of photostriction in ferroelectric perovskite oxides such as bismuth ferrite[52,53] or lead titanate-based compounds[1,54,55], in which large piezoelectric coefficients exist. In this section, we discuss the significance of those mechanisms, and in particular lead an in-depth investigation of the respective contributions of the piezoelectric effect and potential deformation mechanism to the photostriction properties of lead and barium titanate.

A. Estimates of the photo-induced strain in polar phases

Let us now focus on two main mechanisms that have been invoked in ferroelectrics to explain photostriction [3,52,53]: *(i)* the converse piezoelectric effect generated by a photoinduced field, and *(ii)* the electronic pressure created by the redistribution of electrons during excitation.

1. *Piezoelectric contribution*

First, we note that the ionic relaxation occurring under excitation of electrons in the conduction band in our ΔSCF calculations can be translated, to a certain approximation, into a change of polarization $\delta \boldsymbol{P}$, by using the Born effective charge approximation[56] (see Ap-

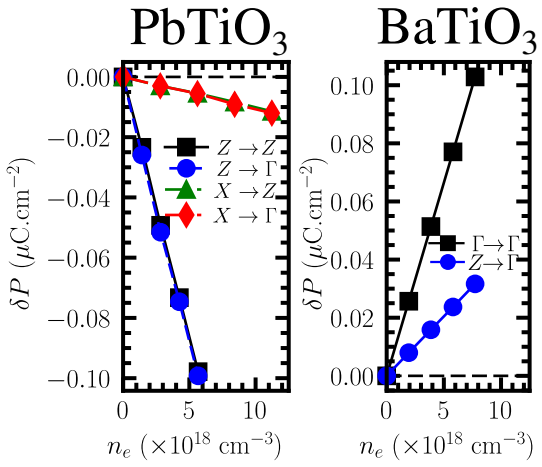

FIG. 10. Change of polarization with the increasing number of photoexcited electrons (left panel) along the tetragonal axis in $P4mm$ lead titanate, and (right panel) along the pseudocubic [001] direction of $R3m$ $BaTiO_3$.

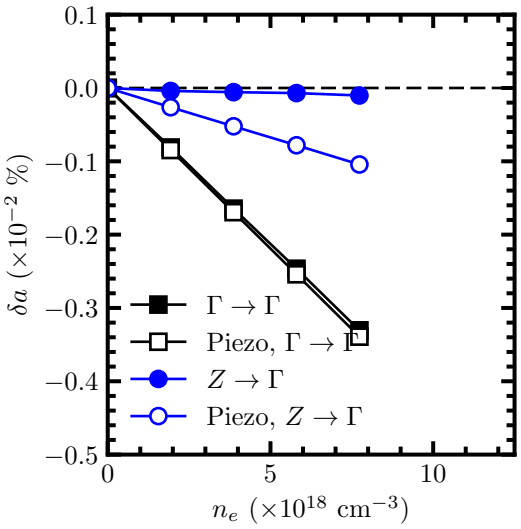

FIG. 11. Change of pseudo-cubic lattice constant in rhombohedral ferroelectric $BaTiO_3$, as calculated in ΔSCF (filled symbols), and as estimated from the converse piezoelectric effect (open symbols).

pendix A for details and discussion about this approximation). One can observe, in Fig. (10), that the total polarization decreases in the case of lead titanate in its $P4mm$ state, while the polarization along the pseudocubic [001] direction of $BaTiO_3$ increases in the polar $R3m$ state. We also note that the absolute rate of change of the polarization is larger for the $Z \to Z$ transition than for the $X \to Z$ transition in lead titanate, and in barium titanate, the $\Gamma \to \Gamma$ transition shows larger rate of change than the $Z \to \Gamma$ one. This hierarchy between the transitions correlates well with the relative magnitudes and signs of the strains photo-induced by different transitions for each material when comparing Fig. (10), and Figs. (3) and (5) respectively. This is the first indication that the piezoelectric effect may largely contribute to the photostriction effect in barium and lead titanates.

In order to gain further quantitative comparison, we note that the change of polarization $\delta\boldsymbol{P}$ can be directly translated into a change of strain $\delta\boldsymbol{\eta}$ through the piezoelectric tensor $\boldsymbol{g}$ (given in Appendix B), as

$$\delta\boldsymbol{\eta} = \boldsymbol{g}.\delta\boldsymbol{P}. \tag{2}$$

Let us start by analyzing the case of barium titanate, plotted in Fig. (11), in which the changes in pseudocubic lattice constant obtained from ΔSCF calculations are shown in filled symbols alongside the estimates (open symbols) resulting from the change of polarization shown in Fig. (10) and the converse piezoelectric effect calculated from Eq. (2). The results are quite satisfying, especially in the case of the $\Gamma \to \Gamma$ transition, while the piezoelectric model tends to slightly overestimate the (weak) rate of change in the case of the $Z \to \Gamma$ transition. Still, the agreement is good, and the piezoelectric model is able to predict that the $Z \to \Gamma$ transition generates a smaller photostrictive effect than the $\Gamma \to \Gamma$ transition.

Let us now move to the $Z \to Z$ and $X \to Z$ transitions in lead titanate, depicted in Figs. (12) & (13). In the case of the $Z \to Z$ transition, the estimates given by the converse piezoelectric effect resulting from a change of the polarization (see Eq. (2), and the corresponding open diamond symbols in Fig. (12)) are in rather good agreement with the calculated values (black squares) for both a and c. In the case of the $X \to Z$ transition, the agreement continues to be good for the lattice constant c along the tetragonal axis (see Fig. (13)). On the other hand, in the left panel of Fig. (13), the lattice constant a in the plane orthogonal to the tetragonal axis is predicted to (slightly) expand using this piezoelectric model, while raw ΔSCF calculations show an opposite behavior. We shall return to that feature in the next section.

2. *Electronic pressure contribution*

It is only natural to wonder whether the other source of photo-induced strain, caused by the electronic pressure mechanism, is the missing part that could explain, for instance, why the piezoelectric model fails to predict the right sign of the photogenerated strain for the a lattice constant for the $X \to Z$ transition in lead titanate. We therefore conducted ΔSCF calculations in $P4mm$ lead titanate, but with frozen atomic positions. In other words, only the cell is allowed to relax. Since atomic coordinates are kept fixed, the ionic contribution to the polarization is (approximately) frozen, and only the effect of the electronic pressure and of the induced electronic dipole (discussed in Appendix A) are accounted for. The results, presented in Figs. (12) and (13) as blue empty circles for

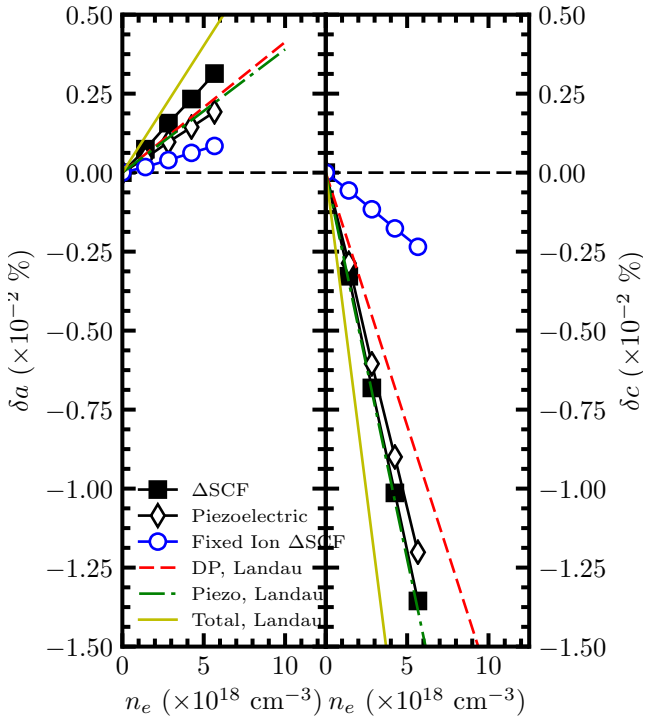

FIG. 12. Relative change of (left panel) basal lattice constant and (right panel) tetragonal lattice constant with increasing concentration of electrons in the conduction band for a $Z \rightarrow Z$ transition in lead titanate, for (filled black squares) ΔSCF calculations, (empty black diamonds) estimates from the change of polarization and the converse piezoelectric effect from Eq. (2), (blue empty circles) ΔSCF calculations with frozen atomic positions, (red dashed line) Deformation Potential in the Landau model, (green dashed dotted line) Piezoelectric effect induced by the photo-induced electric field in the Landau model, (yellow line).

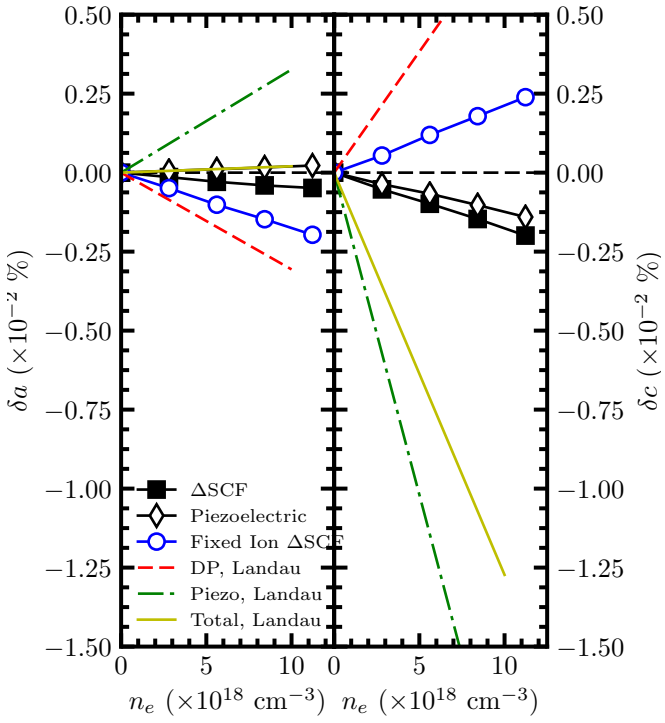

FIG. 13. Relative change of (left panel) basal lattice constant and (right panel) tetragonal lattice constant with increasing concentration of electrons in the conduction band for a $X \rightarrow Z$ transition in $PbTiO_3$, for (filled black squares) ΔSCF calculations, (empty black diamonds) estimates from the change of polarization and the converse piezoelectric effect from Eq. (2), (blue empty circles) ΔSCF calculations with frozen atomic positions, (red dashed line) Deformation Potential in the Landau model, (green dashed dotted line) Piezoelectric effect induced by the photo-induced electric field in the Landau model, (yellow line).

the transitions $Z \rightarrow Z$ and $X \rightarrow Z$ respectively, exhibit marked differences for the two transitions for both the a and c lattice constants. In the case of the $Z \rightarrow Z$ transition, the electronic pressure induces a photogenerated strain that has the same sign than the piezoelectric-induced photo-strain, and thus the two effects *cooperate*. On the other hand, in the case of the $X \rightarrow Z$ transition (see Fig. (13)), the two mechanisms actually *compete*. In particular, for the latter transition, the change of polarization and transverse piezoelectric constant d_{31} are too weak and are overpowered by the deformation potential mechanism, generating a contraction in the plane orthogonal to the tetragonal axis, rather than an expansion.

Overall, one can argue that the photo-induced change of polarization, coupled to the converse piezoelectric effect, is the main mechanism driving photostriction in ferroelectric materials, although the deformation potential mechanism may be significant for some transitions, in particular in directions orthogonal to the polar axis, for which the transverse piezoelectric constants are smaller than the longitudinal ones. For instance, in lead titanate, g_{33} is six times larger than g_{13} (see Appendix B).

B. A Landau approach to photostriction

The model and results described in Section IV.A explicitly take into account the responses of properties (such as polarization or strain) to electrons being ejected into the conduction states and to the existence of holes in the valence states. Let us now investigate if photostriction can also be described by a simpler and original model that consists in focusing on the linear response of some *ground-state* properties and for which the sole contribution of electrons in the conduction states and holes in the valence states resides in their counting. For that, we first recall that the appearance of ferroelectricity upon approaching the paraelectric-to-ferroelectric transition is often described by a phenomenological approach[57–59] involving a thermodynamic potential $\Phi_F(T, \boldsymbol{P}, \boldsymbol{\eta})$ which,

close to the transition, can be expanded in a power series of its order parameters (polarization $\boldsymbol{P}$ and strain $\boldsymbol{\eta}$) with respect to the high-symmetry paraelectric phase,

$$\Phi_F(T,\boldsymbol{P},\boldsymbol{\eta}) = \Phi_P(T) + \frac{\alpha(T)}{2}\boldsymbol{P}^2 + \frac{\beta}{4}\boldsymbol{P}^4 + +\frac{\gamma}{6}\boldsymbol{P}^6 + \frac{C}{2}\boldsymbol{\eta}^2 + \frac{Q}{2}\boldsymbol{P}^2\boldsymbol{\eta}. \quad (3)$$

In the above equation, $\Phi_P(T)$ is the thermodynamic potential of the reference paraelectric phase, $\alpha(T)$ is a temperature-dependent second-rank tensor, β and γ are 4^{th}- and 6^{th}-rank tensors, considered to be temperature independent here. C is the 2^{nd}-rank stiffness tensor, and Q is the 4^{th}-rank electrostrictive tensor. We adopted the short-hand notation $\boldsymbol{P}^n$ to account for the tensorial product $\boldsymbol{P}\otimes\cdots\otimes\boldsymbol{P}$. At equilibrium, the thermodynamic potential must be stationary, and must therefore obey the following equations,

$$\frac{\partial\Phi_F}{\partial\boldsymbol{P}} = 0 = \alpha(T)\boldsymbol{P} + \beta\boldsymbol{P}^3 + \gamma\boldsymbol{P}^5 + Q\boldsymbol{P}\boldsymbol{\eta}, \quad (4)$$

$$\frac{\partial\Phi_F}{\partial\boldsymbol{\eta}} = 0 = C\boldsymbol{\eta} + \frac{1}{2}Q\boldsymbol{P}^2. \quad (5)$$

This set of equations can be solved for $\boldsymbol{P}$ and $\boldsymbol{\eta}$ and yields finite values $\boldsymbol{P}_0$ and $\boldsymbol{\eta}_0$ in the ferroelectric phase, for temperatures below the Curie temperature. So far, no excitation by light has been considered, and it is legitimate to wonder how one can introduce the effect of photoexcitation in this Landau model. Following the pioneering work of Pasynkov[53,60], we add the contribution of the system of free holes and electrons by considering the total thermodynamic potential $\Phi(T,\boldsymbol{P},\boldsymbol{\eta})$

$$\Phi(T,\boldsymbol{P},\boldsymbol{\eta}) = \Phi_F(T,\boldsymbol{P},\boldsymbol{\eta}) + \Phi_{ph}(T,\boldsymbol{P},\boldsymbol{\eta}), \quad (6)$$

with

$$\Phi_{ph}(T,\boldsymbol{P},\boldsymbol{\eta}) = \sum_{n,\boldsymbol{k}} \delta n_{n\boldsymbol{k}}\varepsilon_{n\boldsymbol{k}}. \quad (7)$$

In Eq. (7), $\delta n_{n\boldsymbol{k}}$ is the change of occupancy of the Bloch state $n\boldsymbol{k}$ with respect to the system in the dark, and $\varepsilon_{n\boldsymbol{k}}$ is the energy of that state. Since photon absorption creates the same amount of holes and electrons, the condition $\sum_{n,\boldsymbol{k}}\delta n_{n\boldsymbol{k}} = 0$ must be satisfied. Let us now consider a system in which only two levels, ε_v (a valence band state) and ε_c (a conduction band state), are involved in the absorption process. In that case, Eq. (7) reduces to

$$\Phi_{ph}(T,\boldsymbol{P},\boldsymbol{\eta}) = \delta n_e E_{v\to c}, \quad (8)$$

with δn_e being the number of photoexcited electrons in the conduction band, and $E_{v\to c} = \varepsilon_c - \varepsilon_v$. The latter is a function of temperature, polarization and strain. Assuming that the perturbation induced under illumination is small enough to write $\boldsymbol{P} = \boldsymbol{P}_0 + \delta\boldsymbol{P}$ and $\boldsymbol{\eta} = \boldsymbol{\eta}_0 + \delta\boldsymbol{\eta}$, one can re-write Eq. (8) as a Taylor expansion in terms of $\delta\boldsymbol{P}$ and $\delta\boldsymbol{\eta}$,

$$\Phi_{ph}(T,\boldsymbol{P},\boldsymbol{\eta}) = \Phi_{ph,0} + \delta n_e \left.\frac{\partial E_{v\to c}}{\partial\boldsymbol{\eta}}\right|_{\boldsymbol{P}_0,\boldsymbol{\eta}_0}\delta\boldsymbol{\eta} + \delta n_e \left.\frac{\partial E_{v\to c}}{\partial\boldsymbol{P}}\right|_{\boldsymbol{P}_0,\boldsymbol{\eta}_0}\delta\boldsymbol{P}. \quad (9)$$

In this latter expression, the definition of a photo-induced stress and a photo-induced electric field can immediately be recognized,

$$\boldsymbol{\sigma}_{photo} = -\delta n_e \left.\frac{\partial E_{v\to c}}{\partial\boldsymbol{\eta}}\right|_{\boldsymbol{P}_0,\boldsymbol{\eta}_0} \quad (10)$$

$$\boldsymbol{E}_{photo} = -\delta n_e \left.\frac{\partial E_{v\to c}}{\partial\boldsymbol{P}}\right|_{\boldsymbol{P}_0,\boldsymbol{\eta}_0} \quad (11)$$

The photo-induced stress $\boldsymbol{\sigma}_{photo}$ is generated by the well-known deformation potential mechanism[61,62], in which deformation and electronic density spatial redistribution alter the band structure. Such stress is obviously a source of photo-induced strain, as now the equilibrium conditions for the system under illumination must be written

$$\frac{\partial\Phi}{\partial\boldsymbol{P}} = 0 = \alpha(T)\boldsymbol{P} + \beta\boldsymbol{P}^3 + \gamma\boldsymbol{P}^5 + Q\boldsymbol{\eta}\boldsymbol{P} - \boldsymbol{E}_{photo}, \quad (12)$$

$$\frac{\partial\Phi}{\partial\boldsymbol{\eta}} = 0 = C\boldsymbol{\eta} + \frac{1}{2}Q\boldsymbol{P}^2 - \boldsymbol{\sigma}_{photo}. \quad (13)$$

There is a second, more subtle source of photo-induced strain. The photo-induced electric field $\boldsymbol{E}_{photo}$ generates a shift of the polarization at equilibrium by $\delta\boldsymbol{P}$. This shift couples to the electrostrictive term in Eq. (13), generating another source term of photo-induced strain. Assuming that $\delta\boldsymbol{P}$ and $\delta\boldsymbol{\eta}$ are indeed small responses compared to $\boldsymbol{P}_0$ and $\boldsymbol{\eta}_0$, Eqs. (12-13) can be linearized and solved for $\delta\boldsymbol{P}$ and $\delta\boldsymbol{\eta}$. Remembering that $\boldsymbol{P}_0$ and $\boldsymbol{\eta}_0$ are solutions of Eqs. (4-5), it is found that,

$$\delta\boldsymbol{P} = \chi_{ph}\boldsymbol{E}_{photo} + d_{ph}^T\boldsymbol{\sigma}_{photo}, \quad (14)$$

$$\delta\boldsymbol{\eta} = S_{ph}\boldsymbol{\sigma}_{photo} + d_{ph}\boldsymbol{E}_{photo}. \quad (15)$$

In the latter equations, $\chi_{ph} = \left(\chi_0^{-1} - Q\boldsymbol{P}_0C^{-1}Q\boldsymbol{P}_0\right)^{-1}$ is a modified dielectric susceptibility, while $\chi_0 = \left(\alpha + 3\beta\boldsymbol{P}_0^2 + 5\gamma\boldsymbol{P}_0^4 + Q\eta_0\right)^{-1}$ is the dielectric susceptibility in the dark. Similarly, $S_{ph} = \left(C^{-1} + C^{-1}Q\boldsymbol{P}_0\chi_{ph}Q\boldsymbol{P}_0C^{-1}\right)^{-1}$ is a modified compliance, and $d_{ph} = -C^{-1}Q\boldsymbol{P}_0\chi_{ph}$ is the piezoelectric tensor, modified by illumination. The two previously

Transition	$Z \to Z$	$X \to Z$
$\frac{\partial E_{v\to c}}{\partial \eta_1}$ (eV)	-1.3606	3.4014
$\frac{\partial E_{v\to c}}{\partial \eta_3}$ (eV)	5.4423	-1.3606
$\frac{\partial E_{v\to c}}{\partial P_3}$ (eV.m^2.C^{-1})	2.0581	1.7150

TABLE V. Partial derivatives of $E_{v\to c}$ of different transitions, and estimated photo-induced strain by Deformation Potential (DP) or converse piezoelectric effect (Piezo) from the Landau model.

mentioned terms inducing strain under illumination now appear obvious in Eq. (15).

To be complete, one should also add the energy of the lattice/phonon gas, $\Phi_L = \sum_{n,\boldsymbol{q}} \delta n_{ph,n\boldsymbol{q}} \hbar\omega_{n\boldsymbol{q}}$, in which $\delta n_{ph,n\boldsymbol{q}}$ and $\hbar\omega_{n\boldsymbol{q}}$ represent the change in population and energy of the $n-$th phonon mode at wavevector $\boldsymbol{q}$[9]. This last term accounts for the thermal expansion due to heating of the lattice by electron-phonon interaction. However, DFT calculations are performed at 0 K, and we shall not take that term into account. This can be justified, beyond the mere practical impossibility, by acknowledging that this effect is at most of the same order of magnitude as the potential deformation term[9].

It is interesting to note that the photo-induced strain and electric fields defined in Eqs. (10-11) are directly related to partial derivatives of the difference in monoelectronic energies $E_{v\to c}$ obtained from *ground state* calculations. As a result, there is an easy way of comparing the Landau model detailed in section IV B with ΔSCF calculations. The derivatives of the difference in monoelectronic energies involved were calculated here using the finite difference method, and are reported in Table V, in the case of lead titanate, for the transitions $Z \to Z$ and $X \to Z$.

Using Density Functional Perturbation Theory (DFPT)[63,64], we obtained the elastic constants $S_{11} = 4.997 \times 10^{-3}$ GPa^{-1}, $S_{12} = -8.586 \times 10^{-5}$ GPa^{-1}, $S_{13} = 7.62 \times 10^{-3}$ GPa^{-1}, $S_{33} = 1.665 \times 10^{-3}$ GPa^{-1}, and the piezoelectric constants $d_{33} = -11.88$ pC.N^{-1} and $d_{33} = 74.19$ pC.N^{-1}. From those, we estimated the photo-induced strain resulting from the Landau model (see Eqs. (14,15)), for both the deformation potential mechanism (denoted "DP"; see red dashed line in Figs. (12 & 13)) and the converse piezoelectric effect generated by the photo-induced electric field (denoted "$E_{ph} + Piezo$"; see green dashed-dotted line in Figs. (12 & 13)) in tetragonal lead titanate. Results are also summarized in Table VI. Looking at the separate contributions of the piezoelectric effect and deformation potential in the Landau model, we observe that it qualitatively matches previous conclusions of Section IV.A, that is that the deformation potential cooperates with the piezoelectric effect for the $Z \to Z$ transition, but competes in the case of the $X \to Z$. We also observe that the Landau picture also keeps the relative ordering in terms of magnitude of photo-induced strain between the two transitions, $Z \to Z$ and $X \to Z$. However, it predicts an expansion of the lattice constant a for the $X \to Z$ transition, while ΔSCF calculations indicate that an in-plane contraction should rather occur. In this specific case, the deformation potential and piezoelectric contributions are very close in magnitude, and of opposite sign, and so any small numerical inaccuracy may result in this incorrect prediction. Note also that we used the ground state values of the elastic and piezoelectric constants, while according to Eq. (15), they should be modified under illumination. We must also remark that, for the $X \to Z$ transition, the predicted magnitude of the change of lattice constant c along the tetragonal axis within the Landau model, although qualitatively correct, is much larger than that calculated using ΔSCF.

Overall, this Landau model can be thought as a good preliminary tool to get a qualitative picture of photostriction, and may therefore be suited to quickly screen for efficient photostrictive materials. Nevertheless, the simplicity of this model cannot render some effects inherent to optical excitation, as photo-excited electrons and holes are treated separately as mere dopants. In particular, excitonic effects, caused by the mutual interaction of the photo-excited electron and hole, cannot be properly described in this framework, while ΔSCF calculations can better describe those effects (with more or less accuracy depending on the employed functional). As a result, such Landau model can only be considered as a starting point, and must either be further refined, or be completed with first-principle calculations.

C. Comparison $BaTiO_3$/$PbTiO_3$/$BiFeO_3$

As discussed in the previous section IV A and in Ref.[10], it appears that the photostriction effect in ferroelectrics mainly originates from the converse piezoelectric effect generated by the appearance of a photo-induced electric field, or here, a photo-induced change in polarization[8,10]. Although many experiments have been made on bismuth ferrite, there are better piezoelectric perovskite oxides, in particular solid-solutions using lead titanate, such as relaxor $[Pb(Mg_{1/3}Nb_{2/3})O_3]_{1-x}$-$[PbTiO_3]_x$[14]. It is therefore foreseeable that the photostrictive effect is larger in lead and barium titanates than in bismuth ferrite, as they have larger piezoelectric constants[12,13]. In order to compare these systems, we ran calculations in bismuth ferrite in its $R3c$ ground state with LDA+U ($U = 3.87$ eV[65]) using a plane-wave cut-off of 35 Ha and a $12 \times 12 \times 12$ k-mesh. The transition considered in bismuth ferrite was $Z \to Z$ (see our previous work for a sketch of the band-structure[10]).

It can be seen from Fig. (14) that both barium titanate and lead titanate transitions exhibit larger photostriction than bismuth ferrite, at least for transitions for which the change of polarization is of the same order of magnitude (see Fig. (10)). This confirms that larger piezoelectric constants lead to larger photostrictive effects along

Transition	$\frac{\delta\eta_{DP,1}}{\delta n_e}$	$\frac{\delta\eta_{E_{ph}+Piezo,1}}{\delta n_e}$	$\frac{\delta\eta_{Landau,1}}{\delta n_e}$	$\frac{\delta\eta_{FixedIons,1}}{\delta n_e}$	$\frac{\delta\eta_{\Delta SCF,1}}{\delta n_e}$	$\frac{\delta\eta_{DP,3}}{\delta n_e}$	$\frac{\delta\eta_{E_{ph}+Piezo,3}}{\delta n_e}$	$\frac{\delta\eta_{Landau,3}}{\delta n_e}$	$\frac{\delta\eta_{FixedIons,3}}{\delta n_e}$	$\frac{\delta\eta_{\Delta SCF,3}}{\delta n_e}$
$Z \to Z$	4.13	3.92	8.05	1.51	**5.55**	−16.01	−24.46	−40.41	−4.16	**−24.00**
$X \to Z$	−3.06	3.26	0.20	−1.75	**−0.44**	7.64	−20.38	−16.19	2.15	**−1.75**

TABLE VI. Estimated photo-induced change of strain in tetragonal lead titanate by Deformation Potential (DP) or converse piezoelectric effect (E_{ph}+$Piezo$) as well as their sum ($Landau$) from the Landau model, and comparison with ΔSCF calculations. All values reported are given in $\times 10^{-24}$ cm^{-3}.

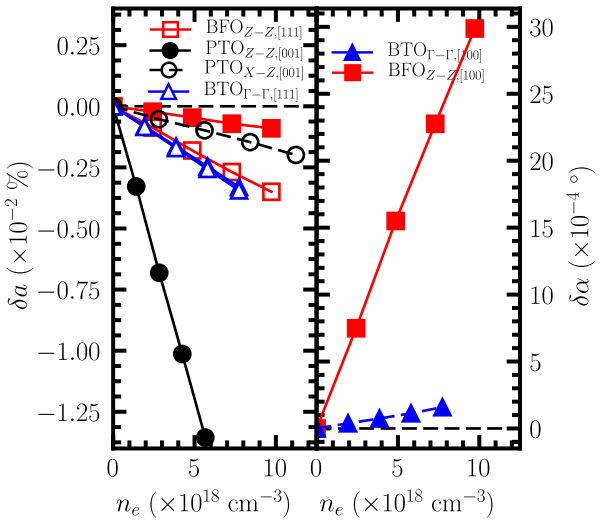

FIG. 14. (left panel) Change of pseudo-cubic lattice constant and (right panel) change of pseudo-cubic angle for different concentrations of photoexcited carriers in $R3c$ $BiFeO_3$ (BFO), $P4mm$ $PbTiO_3$ (PTO) and $R3m$ $BaTiO_3$ (BTO). For PTO, only the change of lattice constant along the tetragonal axis [001] is plotted.

their polar axis (which is along [111] for $BaTiO_3$ and $BiFeO_3$). We note however that, although the pseudocubic change of lattice constant along [100] is much larger in $BaTiO_3$ as compared to $BiFeO_3$, the larger change of pseudocubic angle in BFO causes the shrinking of lattice constant along [111] to be of comparable magnitude for both materials (although still slightly smaller). As far as we are aware of, there are very few works on photostriction in $PbTiO_3$ and $BaTiO_3$, owing to their large bandgap (3.4 eV[66] and 3.3 eV[67]). Most steady photostriction studies have been performed on bismuth ferrite, or in PLZT ceramics[1,68], a compound related to lead titanate. Photo-expansion under UV light of the order of $+2.7 \times 10^{-3}$% was reported along the [101] direction[53] in $BiFeO_3$. According our calculations, an expansion is only possible if this $< 101 >$ direction is actually a $[10\bar{1}]$ direction (i.e., perpendicular to the spontaneous polarization), in which case such expansion would occur for a concentration of photoexcited electrons of roughly 1.6×10^{19} cm^{-3}. According the litterature, concentrations of photo-excited electrons ranging from 5×10^{17} to 5×10^{19} cm^{-3} have been reported[3,69], thus these estimates are in principle reachable to experiments. In the case of PLZT ceramics, photostriction of the order of 10^{-2} % have been achieved[1,68], but those studies seem to indicate an expansion of the material rather than, for instance, the strong decrease that we predict along the tetragonal axis. If we assume that the photostriction measured is along the in-plane lattice constant a, and that all transitions are of the $Z \to Z$ type, that would correspond in our calculation to a concentration of photoexcited carriers of roughly 6.6×10^{19} cm^{-3}. Although this appears large, this can only be taken as a crude estimate, for *(i)* the piezoelectric constant of PLZT at the composition considered (that is in the Morphotropic Phase Boundary) is much larger than that of lead titanate; and *(ii)* the reported experiments were performed in ceramics, which in many regards, differ significantly from a single crystal material. Measurements on single crystals and careful report of the crystallographic directions along which photostriction is measured are thus necessary to allow a direct comparison with the present work.

D. Polaronic effects

This work mainly focuses on the dilute limit. In other words, we do not consider polaronic effects, which require to go to large supercells and to use more elaborate functionals. Polarons, which are made of an electric charge and the surrounding lattice relaxation[70], may alter the relaxation of the lattice under illumination. The LDA functional used in this work does not describe exchange and correlation well enough to properly localize the extra-charge and form a small polaron. Using hybrid functionals such as HSE06, or the LDA+U correction may be solutions, at least to study small hole polarons[40]. Typically, since small hole polarons are not stable in lead titanate[40], we do not expect it to alter the photostriction effect in that material. On the other hand, polarons may be of importance in the relaxation of the lattice under illumination in $BaTiO_3$. How they may impact the photostriction is still an unresolved question, and is the topic of a future work.

V. CONCLUSION

In this work, the ΔSCF method was used to calculate, at a purely *ab-initio* level, photostriction effects in two classical ferroelectric materials, namely barium and

lead titanates. It is found that the pseudo-cubic lattice constant of $R3m$ $BaTiO_3$ shrinks upon increasing the number of photoexcited electrons, and so is the lattice constant of $P4mm$ $PbTiO_3$ along its polar axis, for our considered transitions. Combined with a previous work on bismuth ferrite[10], it therefore appears to be a general trend that directions close or along the polarization shrink upon photoexcitation, as mostly originating from the converse piezoelectric effect generated by the photo-induced change of polarization. In particular, we showed that lead titanate, which has the strongest piezoelectric constant among BTO, PTO and BFO, also exhibits the strongest photostriction effect along the polar axis (for similar photo-induced change of polarization). On the other hand, we showed in the case of lead titanate that, in directions transverse to the polar axis, the deformation potential mechanism becomes more significant, and its competition or cooperation with the piezoelectric mechanism decides whether the photostriction effect is large or not for a particular transition.

Moreover, a transparent and rather straightforward Landau model is developed and presented here. This model is found to provide a simple and fast method to screen for photostrictive materials, based on ground state DFT calculations only. Although its conclusion may so far only be taken as qualitative, further refinements may lead to better quantitative estimates to guide the design of materials with high photostriction conversions.

We therefore hope that the present manuscript is of benefits to the scientific community, and that our predictions will be experimentally confirmed soon.

ACKNOWLEDGMENTS

C.P. and L.B. thank the DARPA grant HR0011-15-2-0038 (MATRIX program). S.P. acknowledges ONR Grant N00014-12-1-1034. S.P appreciates also the grant 3.1649.2017/4.6 of RMES (Russian Ministry of Education and Science). The authors also thank the Arkansas High Performance Computing Center (AHPCC) for computing time and David Chaffin for technical support.

Appendix A: Born charges tensor

In order to access the change of polarization, we computed the Born charges tensor from Density Functional Perturbation Theory, *taking the ferroelectric ground state phase as the reference*. Indeed, the Born charges tensor allows to calculate the change in polarization with respect to a reference configuration,

$$\delta P_\alpha = \frac{e}{V}\sum_{I,\beta} Z_{I,\alpha\beta}\delta u_{I,\beta}, \tag{A1}$$

with e being the elementary charge, $Z_{I,\alpha\beta}$ the Born effective charge tensor of atom I, and $\delta u_{I,\beta}$ the displacement of the I-th atom in direction β with respect to the reference configuration. Since we are interested in change of polarization with respect to the unperturbed ferroelectric ground state in our case, it is only natural to take the latter as the reference state.

Of course, using Born charges is an approximation to compute the polarization, since these charges are typically computed in the ground state while we are dealing here with excited states. However, note that the number of electrons effectively excited is typically of the order of $\frac{1}{N_{k,1}N_{k,2}N_{k,3}}$ where $N_{k,\alpha}$ is the number of k-points in the direction α. Since we use k-meshes which are at least $16\times16\times16$, the number of excited electrons in a unit cell is of the order of 4.8×10^{-4} e. This a very small number. One can also wonder whether the electronic dipole associated with the excitation of the electron-hole pair is important as well. Since the photoexcited electron is located on the titanium , while the photoexcited hole is mostly seating on oxygens as seen from Fig. (4), or projected Density of States or band structures[30], the induced electronic dipole can be estimated as the product of the electronic charge times the relative displacement of the titanium with respect to the oxygen. This, divided by the volume, results in an induced polarization of the order of 2×10^{-3} μC.cm^{-2} and 1×10^{-3} μC.cm^{-2} in lead titanate and barium titanate, for concentration of photoexcited electrons of roughly $7-10\times10^{18}$ cm^{-3}, for which the change of polarization calculated from Born charges is already of the order 10^{-1} μC.cm^{-2} (see Fig. (10)).

Let us now provide the calculated values of the Born effective charge tensor. In the primitive axes of the tetragonal cell of lead titanate, the Born effective charge tensors are given by:

$$Z^*_{Pb} = \begin{pmatrix} 4.0641 & 0 & 0 \\ 0 & 4.0641 & 0 \\ 0 & 0 & 4.0641 \end{pmatrix}, \tag{A2}$$

$$Z^*_{Ti} = \begin{pmatrix} 8.0735 & 0 & 0 \\ 0 & 8.0735 & 0 \\ 0 & 0 & 6.8303 \end{pmatrix}, \tag{A3}$$

$$Z^*_{O_1} = \begin{pmatrix} -2.4581 & 0 & 0 \\ 0 & -5.1882 & 0 \\ 0 & 0 & -2.0071 \end{pmatrix}, \tag{A4}$$

$$Z^*_{O_3} = \begin{pmatrix} -2.0830 & 0 & 0 \\ 0 & -2.0830 & 0 \\ 0 & 0 & -4.3810 \end{pmatrix}, \tag{A5}$$

with O_1 representing an oxygen with coordinates $(1/2, 0, 1/2+\delta z_{O_1})$, and O_3 being an apical oxygen $(1/2, 1/2, \delta z_{O_3})$.

Moreover, in the primitive axes of the $R3m$ rhombohedral cell of barium titanate, we have

$$Z^*_{Ba} = \begin{pmatrix} 2.4255 & -0.0103 & -0.0103 \\ -0.0103 & 2.4255 & -0.0103 \\ -0.0103 & -0.0103 & 2.425 \end{pmatrix}, \quad \text{(A6)}$$

$$Z^*_{Ti} = \begin{pmatrix} 6.7276 & -0.2408 & -0.2408 \\ -0.2408 & 6.7276 & -0.2408 \\ -0.2408 & -0.2408 & 6.7276 \end{pmatrix}, \quad \text{(A7)}$$

$$Z^*_{O_1} = \begin{pmatrix} -1.80487 & -0.00070 & 0.07887 \\ -0.0070 & -1.80487 & 0.07887 \\ 0.1700 & 0.1700 & -4.95047 \end{pmatrix}, \quad \text{(A8)}$$

$$Z^*_{O_2} = \begin{pmatrix} -1.8048 & 0.0788 & -0.0070 \\ 0.1700 & -4.95047 & 0.1700 \\ -0.0070 & 0.07887 & -1.80487 \end{pmatrix}, \quad \text{(A9)}$$

and

$$Z^*_{O_3} = \begin{pmatrix} -4.9505 & 0.1700 & 0.1700 \\ 0.0788 & -1.8048 & -0.0070 \\ 0.0788 & -0.0070 & -1.8048 \end{pmatrix}, \quad \text{(A10)}$$

with $O_1 = (1/2 + \delta x_O, \delta z_O, 1/2 + \delta x_O)$, $O_2 = (\delta z_O, 1/2 + \delta x_O, 1/2 + \delta x_O)$ and $O_3 = (1/2 + \delta x_O, 1/2 + \delta x_O, \delta z_O)$.

Appendix B: Piezoelectric Tensor

Let us also provide the elements of the piezoelectric tensors we computed. In tetragonal lead titanate, the calculated piezoelectric tensor is, in the primitive axes,

$$\boldsymbol{g}_{PTO} = \begin{pmatrix} 0 & 0 & -0.01966 \\ 0 & 0 & -0.01966 \\ 0 & 0 & 0.12280 \\ 0 & 0.04687 & 0 \\ 0.04687 & 0 & 0 \\ 0 & 0 & 0 \end{pmatrix} \text{ m}^2.\text{C}^{-1}. \quad \text{(B1)}$$

In barium titanate, in the primitive rhombohedral axes, the tensor is

$$\boldsymbol{g}_{BTO} = \begin{pmatrix} -0.06000 & 0.01351 & 0.01351 \\ 0.01351 & -0.06000 & 0.01351 \\ 0.01351 & 0.01351 & -0.06000 \\ 0.00031 & -0.00954 & -0.00954 \\ -0.00954 & 0.00031 & -0.00954 \\ -0.00954 & -0.00954 & 0.00031 \end{pmatrix} \text{ m}^2.\text{C}^{-1}. \quad \text{(B2)}$$

[1] K. Uchino, Materials Research Innovations **1**, 163 (1997).
[2] P. Ruello, T. Pezeril, S. Avanesyan, G. Vaudel, V. E. Gusev, I. C. Infante, and B. Dkhil, Applied Physics Letters **100**, 212906 (2012).
[3] M. Lejman, G. Vaudel, I. C. Infante, P. Gemeiner, V. E. Gusev, B. Dkhil, and P. Ruello, Nature Communications **5**, 4301 (2014).
[4] M. Lejman, G. Vaudel, I. C. Infante, I. Chaban, T. Pezeril, M. Edely, G. F. Nataf, M. Guennou, J. Kreisel, V. E. Gusev, B. Dkhil, and P. Ruello, Nature Communications **7**, 12345 (2016).
[5] Y. Li, C. Adamo, P. Chen, P. G. Evans, S. M. Nakhmanson, W. Parker, C. E. Rowland, R. D. Schaller, D. G. Schlom, D. a. Walko, H. Wen, and Q. Zhang, Scientific Reports **5**, 16650 (2015).
[6] H. Lu, C.-W. Bark, D. Esque de los Ojos, J. Alcala, C. B. Eom, G. Catalan, and A. Gruverman, Science **336**, 59 (2012).
[7] V. Iurchuk, D. Schick, J. Bran, D. Colson, A. Forget, D. Halley, A. Koc, M. Reinhardt, C. Kwamen, N. A. Morley, M. Bargheer, M. Viret, R. Gumeniuk, G. Schmerber, B. Doudin, and B. Kundys, Physical Review Letters **117**, 107403 (2016).
[8] B. Kundys, Applied Physics Reviews **2**, 011301 (2015).
[9] C. Thomsen, H. T. Grahn, H. J. Maris, and J. Tauc, Physical Review B **34**, 4129 (1986).
[10] C. Paillard, B. Xu, B. Dkhil, G. Geneste, and L. Bellaiche, Physical Review Letters **116**, 247401 (2016).
[11] M. Graf, M. Sepliarsky, R. Machado, and M. Stachiotti, Solid State Communications **218**, 10 (2015).
[12] D. Lebeugle, D. Colson, A. Forget, M. Viret, P. Bonville, J. F. Marucco, and S. Fusil, Physical Review B **76**, 024116 (2007).
[13] D. Berlincourt and H. Jaffe, Physical Review **111**, 143 (1958), arXiv:arXiv:1011.1669v3.
[14] T. R. Shrout, Z. P. Chang, N. Kim, and S. Markgraf, Ferroelectrics Letters Section **12**, 63 (1990).
[15] R. Haleoot, C. Paillard, M. Mehboudi, B. Xu, L. Bellaiche, and S. Barraza-Lopez, , 1 (2017), arXiv:1701.02249.
[16] P. Hohenberg and W. Kohn, Physical Review **136**, B864 (1964).
[17] W. Kohn and L. J. Sham, Physical Review **140**, A1133 (1965).
[18] R. M. Martin, *Electronic Structure: Basic Theory and Practical Methods* (Cambridge University Press, Cambridge, England, 2004).
[19] J. Gavnholt, T. Olsen, M. Engelund, and J. Schiøtz, Physical Review B **78**, 075441 (2008), arXiv:arXiv:0807.3242v1.
[20] K. Nakamura, Y. Kitaoka, T. Akiyama, T. Ito, M. Weinert, and A. J. Freeman, Physical Review B **85**, 235129 (2012).
[21] J. P. Perdew, International Journal of Quantum Chemistry **30**, 451 (1986).
[22] L. Hedin, Physical Review **139**, A796 (1965), arXiv:9712013v1 [arXiv:cond-mat].

[23] C. A. Ullrich, *Time-Dependent Density-Functional Theory, Concepts and Applications* (Oxford University Press, 2012).

[24] J. Deslippe, G. Samsonidze, D. A. Strubbe, M. Jain, M. L. Cohen, and S. G. Louie, Computer Physics Communications **183**, 1269 (2012), arXiv:1111.4429.

[25] X. Gonze, B. Amadon, P.-M. Anglade, J.-M. Beuken, F. Bottin, P. Boulanger, F. Bruneval, D. Caliste, R. Caracas, M. Côté, T. Deutsch, L. Genovese, P. Ghosez, M. Giantomassi, S. Goedecker, D. Hamann, P. Hermet, F. Jollet, G. Jomard, S. Leroux, M. Mancini, S. Mazevet, M. Oliveira, G. Onida, Y. Pouillon, T. Rangel, G.-M. Rignanese, D. Sangalli, R. Shaltaf, M. Torrent, M. Verstraete, G. Zerah, and J. Zwanziger, Computer Physics Communications **180**, 2582 (2009).

[26] P. E. Blöchl, Physical Review B **50**, 17953 (1994).

[27] M. Torrent, F. Jollet, F. Bottin, G. Zérah, and X. Gonze, Computational Materials Science **42**, 337 (2008).

[28] J. P. Perdew and Y. Wang, Physical Review B **46**, 12947 (1992).

[29] A. García and D. Vanderbilt, Physical Review B **54**, 3817 (1996).

[30] P. Ghosez, X. Gonze, and J. P. Michenaud, Ferroelectrics **220**, 1 (1999).

[31] Y. Zhou, L. You, S. Wang, Z. Ku, H. Fan, D. Schmidt, A. Rusydi, L. Chang, L. Wang, P. Ren, L. Chen, G. Yuan, L. Chen, and J. Wang, Nature Communications **7**, 11193 (2016).

[32] B. Meyer and D. Vanderbilt, Physical Review B **65**, 104111 (2002).

[33] G. Sághi-Szabó, R. E. Cohen, and H. Krakauer, Physical review letters **80**, 4321 (1998).

[34] T. Shimada, T. Ueda, J. Wang, and T. Kitamura, Physical Review B **87**, 1 (2013).

[35] G. Shirane, R. Pepinsky, and B. C. Frazer, Acta Crystallographica **9**, 131 (1956).

[36] J. W. Edwards, R. Speiser, and H. L. Johnston, Journal of the American Chemical Society **73**, 2934 (1951).

[37] G. Shirane and S. Hoshino, Journal of the Physical Society of Japan **6**, 265 (1951).

[38] G. H. Kwei, A. C. Lawson, S. J. L. Billinge, and S. W. Cheong, The Journal of Physical Chemistry **97**, 2368 (1993).

[39] W. Setyawan and S. Curtarolo, Computational Materials Science **49**, 299 (2010), arXiv:1004.2974.

[40] P. Erhart, A. Klein, D. Åberg, and B. Sadigh, Physical Review B **90**, 035204 (2014), arXiv:arXiv:1402.0435v1.

[41] D. Daranciang, M. J. Highland, H. Wen, S. M. Young, N. C. Brandt, H. Y. Hwang, M. Vattilana, M. Nicoul, F. Quirin, J. Goodfellow, T. Qi, I. Grinberg, D. M. Fritz, M. Cammarata, D. Zhu, H. T. Lemke, D. Walko, E. M. Dufresne, Y. Li, J. Larsson, D. a. Reis, K. Sokolowski-Tinten, K. a. Nelson, A. M. Rappe, P. H. Fuoss, G. B. Stephenson, and A. M. Lindenberg, Physical Review Letters **108**, 087601 (2012).

[42] H. Wen, P. Chen, M. P. Cosgriff, D. Walko, J. Lee, C. Adamo, R. D. Schaller, J. Ihlefeld, E. M. Dufresne, D. G. Schlom, P. Evans, J. Freeland, and Y. Li, Physical Review Letters **110**, 037601 (2013).

[43] D. Schick, M. Herzog, H. Wen, P. Chen, C. Adamo, P. Gaal, D. G. Schlom, P. G. Evans, Y. Li, and M. Bargheer, Physical Review Letters **112**, 097602 (2014).

[44] H. Wen, M. Sassi, Z. Luo, C. Adamo, D. G. Schlom, K. M. Rosso, and X. Zhang, Scientific Reports **5**, 15098 (2015).

[45] J. P. Perdew, A. Ruzsinszky, G. I. Csonka, O. A. Vydrov, G. E. Scuseria, L. A. Constantin, X. Zhou, and K. Burke, Physical Review Letters **100**, 136406 (2008), 0707.2088.

[46] V. M. Fridkin and B. N. Popov, Soviet Physics Uspekhi **981** (1978).

[47] V. M. Fridkin, E. P. Efremova, B. H. Karimov, V. A. Kuznezov, I. P. Kuzmina, A. N. Lobachev, V. G. Lazarev, and A. J. Rodin, Applied Physics **25**, 77 (1981).

[48] B. I. Sturman and V. M. Fridkin, *The Photovoltaic and Photorefractive Effects in Noncentrosymmetric Materials* (Gordon and Breach Science Publishers, 1992).

[49] V. M. Fridkin, Crystallography Reports **46**, 654 (2001).

[50] C. Paillard, X. Bai, I. C. Infante, M. Guennou, G. Geneste, M. Alexe, J. Kreisel, and B. Dkhil, Advanced Materials **28**, 5153 (2016).

[51] P. Lopez-Varo, L. Bertoluzzi, J. Bisquert, M. Alexe, M. Coll, J. Huang, J. A. Jimenez-Tejada, T. Kirchartz, R. Nechache, F. Rosei, and Y. Yuan, Physics Reports **653**, 1 (2016).

[52] B. Kundys, M. Viret, D. Colson, and D. O. Kundys, Nature materials **9**, 803 (2010).

[53] B. Kundys, M. Viret, C. Meny, V. Da Costa, D. Colson, and B. Doudin, Physical Review B **85**, 092301 (2012).

[54] S.-Y. Chu, Z. Ye, and K. Uchino, Advanced Performance Materials **1**, 129 (1994).

[55] P. Poosanaas and K. Uchino, Materials chemistry and physics **61**, 36 (1999).

[56] R. Resta and D. Vanderbilt, in *Physics of Ferroelectrics*, Vol. 105 (Springer Berlin Heidelberg, Berlin, Heidelberg, 2007) pp. 31–68.

[57] L. Landau and E. Lifshitz, *Course of Theoretical Physics Vol. 5: Statistical Physics*, 2nd ed. (Pergamon Press, 1970).

[58] A. Devonshire, The London, Edinburgh, and Dublin Philosophical Magazine and Journal of Science **40**, 1040 (1949).

[59] C. Kittel, *Introduction to Solid State Physics*, 8th ed. (Wiley, New York, 2004) p. 703.

[60] R. E. Pasynkov, Ferroelectrics **6**, 19 (1973).

[61] J. Bardeen and W. Shockley, Physical Review **80**, 72 (1950).

[62] C. Herring and E. Vogt, Physical Review **101**, 944 (1956).

[63] X. Gonze, Physical Review B **55**, 10337 (1997).

[64] X. Gonze and C. Lee, Physical Review B **55**, 10355 (1997).

[65] S. Lisenkov, I. Kornev, and L. Bellaiche, Physical Review B **79**, 012101 (2009).

[66] J. F. Scott, *Ferroelectric Memories*, Springer Series in Advanced Microelectronics, Vol. 3 (Springer Berlin Heidelberg, Berlin, Heidelberg, 2000) p. 248.

[67] S. Sanna, C. Thierfelder, S. Wippermann, T. P. Sinha, and W. G. Schmidt, Physical Review B **83**, 054112 (2011).

[68] X. Wang, J. Huang, J. Wang, and H. Yue, International Journal of Applied Electromagnetics and Mechanics **46**, 965 (2014).

[69] K. Prashanthi, P. Dhandharia, N. Miriyala, R. Gaikwad, D. Barlage, and T. Thundat, Nano Energy **13**, 240 (2015).

[70] D. Emin, *Polarons* (Cambridge University Press, Cambridge, England, 2013) p. 227.